Applications and Applied Mathematics: An International Journal (AAM)

Volume 16 | Issue 1 Article 39

6-2021

Thermal-Diffusion and Diffusion-Thermo Effects on Heat and Mass Transfer in Chemically Reacting MHD Casson Nanofluid with Viscous Dissipation

Timothy L. Oyekunle
University of Ilorin

Mojeed T. Akolade
University of Ilorin

Samson A. Agunbiade
University of Ilorin

Available at
http://pvamu.edu/aam
Appl. Appl. Math.
ISSN: 1932-9466

Applications and Applied Mathematics:
An International Journal
(AAM)

Vol. 16, Issue 1 (June 2021), pp. 705 – 723

Thermal-Diffusion and Diffusion-Thermo Effects on Heat and Mass Transfer in Chemically Reacting MHD Casson Nanofluid with Viscous Dissipation

[1]Timothy L. Oyekunle, [2*]Mojeed T. Akolade, and [3]Samson A. Agunbiade

Department of Mathematics
Faculty of Physical Sciences
University of Ilorin
Ilorin, Nigeria
[1]tloyekunle95@gmail.com; [2]17-68ev006pg@students.unilorin.edu.ng;
[3]agunbiade1971@gmail.com

*Corresponding author

Received: August 7, 2020; Accepted: March 9, 2021

Abstract

In this paper, we examined the combined effects of dissipation and chemical reaction in Casson nanofluid motion through a vertical porous plate subjected to the magnetic field effect placed perpendicular to the flow channel. The physical problem is modeled using partial differential equations (PDEs). These sets of PDEs, with suitable similarity transformations, are simplified into ordinary differential equations (ODEs). Collocation technique with legendary basis function is utilized in solving the transformed equations. The numerical analysis on velocity, concentration, and temperature are plotted and tabled for different flow parameters. Our findings show that by raising the Casson parameter close to infinity, the behavior of Casson fluid obeys the law of viscosity. Conversion of energy via the work done by the fluid molecules, influences both dimensionless velocity and temperature profiles significantly, while the mass flux hikes the concentration profile. The heat generated by the intermolecular reaction of fluid particles resulted in a large amount of heat produced in the flow field.

Keywords: Casson nanofluid; Thermal-diffusion; Diffusion-thermo; Collocation method; Legendary Polynomial

MSC 2010 No.: 65L60, 76A05, 76M55, 76W05

1. Introduction

Heat and mass transfer over a flat surface has been analyzed by many researchers in recent times, considering its applications in engineering and industries. In the convective heat and mass transfer, the buoyancy forces emanating from the integration of species diffusion and thermal play a vital role in the simultaneously physical processes such as in polymer production, food processing industries, drying the wet surface of a body by evaporation and transfer of energy in a wet cooling tower. Others include formation and depression of fog, chemical distillation process, design of heat exchangers, among others (Rajasekhar et al. (2013)). A non-Newtonian fluid such as Casson has also been frequently investigated due to its outspread request in pharmaceutical, chemical, and cosmetic industries which can be seen in the manufacturing of chemicals, china clay, paints, syrup, gas, cleanser, juice, among others (Jawad et al. (2016) and Chaoyang et al. (1989)).

Due to the novel applications of the considered fluid (Casson nanofluid), mass and heat flow processes, researchers like Oyelakin et al. (2016) account for the influence of Soret and Dufour while investigating the flow of Casson nanofluid with radiation impact past a stretching sheet. They reported that the effect of the Casson parameter slows down the velocity and temperature growth. Haroun et al. (2015) examined the MHD effect in the flow of mass and heat transfer with the mixed convective flow of a nanofluid. Nanofluid investigation through an impulsive and radiating flow was presented by Turkyilmazoglu (2015). Raju et al. (2016) presented the analysis of thermal radiation and chemical reaction on Casson fluid flow past an exponentially surface. It is discovered that a hike in the heat source number diminished the energy field. The study over an inclined plate, non-Newtonian nanofluid and double-diffusive effects, numerical investigation of the flow are carried out by Rafique et al. (2019) via the Keller Box method, while Idowu et al. (2020a) combined the double-diffusive effect with thermophoresis influence on the flow of MHD Casson fluid rheology. It is reported that an increase in the Casson nanofluid parameter gave rise to the skin friction and slow down the energy and concentration profiles accordingly.

Thermo-physical effects on the free convective flow of MHD Casson dissipative fluid were investigated by Idowu et al. (2020b), where a modified heat flux model was employed. The result shows that a hike in Casson number downsized the fluid momentum and concentration fields, while temperature gave a contrary behavior. Uddin et al. (2012) highlighted the effect of Newtonian nanofluid on free convective and MHD boundary layer flow subjected to convective heating boundary conditions, they discovered that temperature and velocity profiles rise with Newtonian heating parameter. Gbadeyan et al. (2020) looked into the influence of variable viscosity and thermal conductivity on Casson nanofluid flowing with velocity slip and convective heating impact. They deduced that a rise in the Casson number speeds up the flow momentum and slow down the temperature field. MHD impact in the movement of Casson fluid includes Idowu et al. (2020c) investigation through the annular medium, Akolade et al. (2020) study of squeezing flow in vertical channel, solutions of rotating disk examination by Turkyilmazoglu (2010) and Turkyilmazoglu (2012), Closed-form solutions of convection flow in porous media by

Turkyilmazoglu (2019). Impact of chemical reaction on MHD flow Casson nanofluid with nonlinear radiative influence and heat transfer is presented by Gireesha et al. (2018) and reported that Casson fluid tends to ride the flow process rapidly.

The mass flux generated by temperature gradient known as thermal-diffusion (Soret) is considered useful in the mixture of gases with medium molecular weight (Nitrogen-air) and very light molecular weight (Hydrogen-Helium). The energy flux generated by composition gradients known as Diffusion-thermo (Dufour) is also considered useful in the isotope separation among others. Therefore, the relationship between the driven potential and corresponding fluxes are of importance in the simultaneous occurrence of heat and mass transfer in a flowing fluid (Kafoussias et al. (1995)). Because of these technological applications of the terms in sciences and engineering, Ullah et al. (2017) analyzed the effects of thermal-diffusion and diffusion-thermo on unsteady mixed convection slip flow of Casson fluid over a nonlinearly stretching sheet and noticed that diffusion-thermo influence on temperature is more pronounced compared with thermal-diffusion. Raju et al. (2016) present double diffusive effects on unsteady heat and mass transfer in an electrically conducting natural convection Couette flow. They observed that the rate of heat transfer coefficient and temperature profile increases with a rise in the Dufour parameter.

Furthermore, the effect of Soret-Dufour on heat and mass transfer of boundary layer flow over a porous wedge with thermal radiation is investigated by Alao et al. (2019). Gbadeyan et al. (2018) analyzed the Soret-Dufour effect on heat and mass transfer in chemically reacting MHD flow through a wavy channel. The effects of Soret and Dufour between two rectangular plane walls with heat source/sink is investigated by (Ali et al. (2016), Ali et al. (2019)) and reported that an increase in Dufour and Soret number reduced the concentration distributions and accelerated the temperature. Other literature on two-diffusive effects with mass and heat transfer in different geometries includes Arthur et al. (2015), Kaladhar et al. (2019), Akolade et al. (2021), and Idowu and Falodun (2019).

The main focus of the present investigation is to explore the influence of dissipation, thermal-diffusion, Diffusion-thermo, and thermal radiation on heat and mass transfer motion in chemically reacting MHD Casson nanofluid with convective heating, to authors knowledge the flow problem is yet to be given consideration.

2. Mathematical Analysis

An electrically conducting, incompressible, laminar, and free convective flow of steady and two-dimensional movement of Casson nanofluid embedding dissipation and chemical reaction through a vertical plate is investigated. The *x*-axis taken parallel to the plate which is in the direction of the flow field, and *y*-axis assumed perpendicular to it (see Figure 1). We neglected the induced magnetic field generated, as it is assumed small. Therefore, the magnetic field $B(\bar{x}) = {}^{B_0}\!\!\diagup\!\!_{\bar{x}^{\frac{1}{2}}}$ with

variable electrical field effect $\sigma^* = \sigma_0 \bar{u}$, where σ_0, B_0 represents the constant electrical and magnetic field influence respectively is been applied normally to the fluid flow direction. The surface of the plate and ambient temperatures are taken to be T_f and T_∞ accordingly, while the wall and ambient mass transfer are taken to be C_w and C_∞ respectively. The Rheological equations of Casson fluid are assumed: ((Idowu et al. (2020b) and Gbadeyan et al. (2020)),

$$\tau_{ij} = \begin{cases} 2\left(\mu B + \dfrac{P_y}{\sqrt{2\pi}}\right) e_{ij}, \pi > \pi_c, \\ 2\left(\mu B + \dfrac{P_y}{\sqrt{2\pi_c}}\right) e_{ij}, \pi < \pi_c, \end{cases} \tag{1}$$

$$P_y = \frac{\mu B \sqrt{2\pi}}{\alpha}, \tag{2}$$

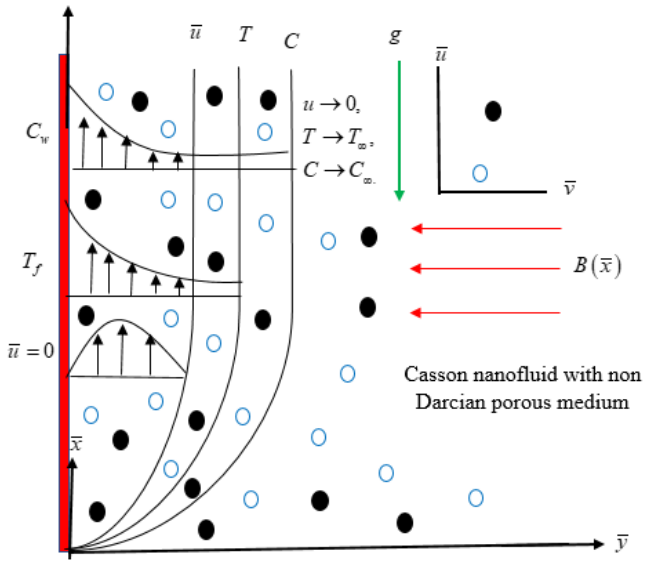

Figure 1: Geometry of Casson nanofluid with non Darcian porous medium.

where $\tau_{ij}, P_y, \mu B, \alpha, e_{ij} \pi = e_{ij} e_{ij}$ and π_c are stress tensor, fluid yield stress, dynamic viscosity, Casson parameter, rate of the strain tensor, the product of the rate of strain tensors, and critical value for the model respectively. The velocities along $\bar{x}$ and $\bar{y}$ directions are denoted by $\bar{u}$ and $\bar{v}$ respectively. The temperature and concentration of the fluid are respectively taken as T and C.

Based on the above assumption, boundary layer, and Boussinesq approximation theory, the Casson nanofluid motion is governed by the following flow model equations (Animasaun (2015) and

Gbadeyan et al. (2020)).

$$\frac{\partial \bar{v}}{\partial \bar{y}} + \frac{\partial \bar{u}}{\partial \bar{x}} = 0 , \tag{3}$$

$$\rho_f \left(\bar{v}\frac{\partial \bar{u}}{\partial \bar{y}} + \bar{u}\frac{\partial \bar{u}}{\partial \bar{x}} \right) = \mu\left(1+\alpha^{-1}\right)\frac{\partial^2 \bar{u}}{\partial \bar{y}^2} - g\left[(\rho_p - \rho_{f_\infty})(C - C_\infty) - \rho_{f_\infty}\beta_0(1+C_\infty)(T - T_\infty) \right] - \sigma_0 B^2(\bar{x})\bar{u}^{-2} - \frac{\mu\left(1+\alpha^{-1}\right)}{k_p}\bar{u} - \frac{b^*}{k_p}\bar{u}^{-2}, \tag{4}$$

$$\bar{v}\frac{\partial T}{\partial \bar{y}} + \bar{u}\frac{\partial T}{\partial \bar{x}} = \alpha^*\frac{\partial^2 T}{\partial \bar{y}^2} + \tau\left[\frac{D_T}{T_\infty}\left(\frac{\partial T}{\partial \bar{y}}\right)^2 + D_B\frac{\partial C}{\partial \bar{y}}\frac{\partial T}{\partial \bar{y}} \right] - \frac{1}{\rho_f c_p}\frac{\partial q_r}{\partial \bar{y}} + Q + \frac{D_m k_0}{c_s c_p}\frac{\partial^2 C}{\partial \bar{y}^2} + \frac{\mu\left(1+\alpha^{-1}\right)}{\rho_f c_p}\left(\frac{\partial \bar{u}}{\partial \bar{y}}\right)^2, \tag{5}$$

$$\bar{v}\frac{\partial C}{\partial \bar{y}} + \bar{u}\frac{\partial C}{\partial \bar{x}} = D_B\frac{\partial^2 C}{\partial \bar{y}^2} - k^*(C - C_\infty) + \frac{D_T}{T_\infty}\frac{\partial^2 T}{\partial \bar{y}^2} + \frac{D_m k_0}{T_m}\frac{\partial^2 T}{\partial \bar{y}^2}, \tag{6}$$

with the boundary conditions

$$\begin{cases} \bar{u} = 0, -k\dfrac{\partial T}{\partial \bar{y}} = h_f(\bar{x})(T_f - T),\ C = C_w,\ at\ \bar{y} = 0, \\ \bar{u} = 0,\ T \to T_\infty, C \to C_\infty\ as\ \bar{y} \to \infty. \end{cases} \tag{7}$$

where α stand for Casson parameter, $\tau = \dfrac{(\rho_c)_p}{(\rho_c)_f}$ and $\alpha^* = \dfrac{k}{(\rho_c)_f}$ are ratios of the nanoparticle to base fluid heat capacity, and the thermal diffusivity of the fluid respectively. Representation of other terms in equations (3) - (7) include ρ_f which is the fluid density, β_0 denoted volumetric thermal expansion, σ_0 is the constant electric conductivity, B_0 denoted constant magnetic field, ρ_p represents the density of nanofluid, b^* is the Forchheimer's initial coefficient, $h_f(\bar{x})$ is the heat transfer coefficient, c_p is the specific heat capacity, D_m denoted Brownian coefficient, c_s represents the absorption susceptibility D_B is the mass diffusion coefficient, k^* denoted constant rate of chemical reaction, k_0 denoted fluid thermal-diffusion ratio, μ represent the constant coefficient of viscosity, κ represents the constant coefficient of thermal conductivity, T_m is the mean fluid temperature, ρ_p represents the density of nanoparticle, ρ_{f_∞} density of the base fluid at the free stream, D_T denoted thermophoresis coefficient, g represents acceleration due to gravity, k_p denoted porous medium permeability and k represents thermal conductivity,

The radiative heat flux q_r using Rossland approximation for diffusion is given as

$$q_r = \frac{4\sigma_1}{3k_1}\frac{\partial T^4}{\partial \bar{y}}, \tag{8}$$

where k_1 is the Rossland mean absorption constant, and σ_1 is the Stefan-Boltzmann number. Taken temperature difference to be sufficiently small within the flow and expand T^4 using Taylor series expansion gives

$$T^4 = 4T_\infty^3 T - 3T_\infty^4 . \tag{9}$$

The darcy Forchheimer model over a vertical plate is subjected to heat generation/absorption of the form

$$Q = \frac{Q_1}{\rho_f c_p}\left(T - T_\infty\right), \tag{10}$$

where Q_1 is the heat source parameter. We introduced the following non-dimensional variables into the dimensional governing equations (3)–(7) to give the equations in non-dimensional form

$$x = \frac{\bar{x}}{L},\ y = \frac{\bar{y}Ra^{\frac{1}{4}}}{L},\ u = \frac{\bar{u}L}{\alpha^* Ra^{\frac{1}{2}}},\ v = \frac{\bar{v}L}{\alpha^* Ra^{\frac{1}{4}}},\ \phi = \frac{C - C_\infty}{C_w - C_\infty},\ \theta = \frac{T - T_\infty}{T_f - T_\infty}. \tag{11}$$

Thus, the dimensionless equations are as follows;

$$v\frac{\partial u}{\partial y} + u\frac{\partial u}{\partial x} = P_r\left(1+\alpha^{-1}\right)\left[\frac{\partial^2 u}{\partial y^2} - \frac{L^2}{k_p Ra^{\frac{1}{2}}}u\right] + P_r\left(\theta - N_r\phi\right) - \frac{H}{x}u^2 - \frac{b^* L}{k_p}u^2, \tag{12}$$

$$v\frac{\partial \theta}{\partial y} + u\frac{\partial \theta}{\partial x} = \frac{\partial^2 \theta}{\partial y^2} + Nb\frac{\partial \phi}{\partial y}\frac{\partial \theta}{\partial y} + Nt\left(\frac{\partial \theta}{\partial y}\right)^2 + R\frac{\partial^2 \theta}{\partial y^2} + G\theta + Df\frac{\partial^2 \phi}{\partial y^2} + P_r Ec\left(1+\alpha^{-1}\right)\left(\frac{\partial u}{\partial y}\right)^2, \tag{13}$$

$$v\frac{\partial \phi}{\partial y} + u\frac{\partial \phi}{\partial x} = \left(\frac{Nt}{Nb}\frac{1}{Le} + Sr\right)\frac{\partial^2 \theta}{\partial y^2} + \frac{1}{Le}\frac{\partial^2 \phi}{\partial y^2} - \gamma\phi, \tag{14}$$

subjected to

$$\begin{cases} u=0,\ \ \dfrac{\partial\theta}{\partial y}=-\dfrac{Lh_f(x)}{kRa^{\frac{1}{4}}}(1-\theta),\ \phi=1\ \ at\ \ y=0, \\ u\to 0,\ \theta\to 0,\ \ \phi\to 0,\ \ as\ \ \ y\to\infty, \end{cases} \tag{15}$$

where

$$H=\frac{\sigma_0 B_0^2}{\rho_f},\ Nr=\frac{(\rho_p-\rho_{f_\infty})(C_w-C_\infty)}{\rho_{f_\infty}B_0(T_f-T_\infty)(1-C_\infty)},\ \Pr=\frac{\nu}{\alpha^*},\ Nb=\frac{\tau D_B(C_w-C_\infty)}{\alpha^*},Nt=\frac{\tau D_t(T_f-T_\infty)}{T_\infty\alpha^*}$$
$$G=\frac{L^2Q_1}{\alpha^* Ra^{\frac{1}{2}}\rho_f C_p},Df=\frac{D_m k_0(C_w-C_\infty)}{\alpha^* C_s C_p(T_f-T_\infty)},Le=\frac{\alpha^*}{D_B},\gamma=\frac{k^*L^2}{\alpha^* Ra^{\frac{1}{2}}},R=\frac{16\sigma_1 T_\infty^3}{3k_1 k},Sr=\frac{D_m k_0(T_f-T_\infty)}{T_m\alpha^*(C_w-C_\infty)}. \tag{16}$$

From equation (16), Nt is the thermophoresis parameter, Nb is the Brownian motion number, H is the magnetic field parameter, $\Pr$ is the Prandtl number, Nr is the buoyancy ratio parameter, G is the heat source parameter, Df is the diffusion-thermo parameter, Ec is the Eckert number, γ is the chemical reaction parameter, R is the radiation parameter, Sr is the thermal-diffusion parameter, and Ra represents the Rayleigh number, and Le is the Lewis number.

Introducing $u=\dfrac{\partial\psi}{\partial y},v=-\dfrac{\partial\psi}{\partial x}$ into equations (12)–(15) gives

$$\frac{\partial\psi}{\partial y}\frac{\partial^2\psi}{\partial x\partial y}-\frac{\partial\psi}{\partial x}\frac{\partial^2\psi}{\partial y^2}=\Pr\left(1+\alpha^{-1}\right)\left[\frac{\partial^3\psi}{\partial y^3}-\frac{L^2}{k_p Ra^{\frac{1}{2}}}\frac{\partial\psi}{\partial y}\right]+\Pr(\theta-Nr\phi)-\frac{H}{x}\left(\frac{\partial\psi}{\partial y}\right)^2-\frac{b^*L}{k_p}\left(\frac{\partial\psi}{\partial y}\right)^2, \tag{17}$$

$$\frac{\partial\psi}{\partial y}\frac{\partial\theta}{\partial x}-\frac{\partial\psi}{\partial x}\frac{\partial\theta}{\partial y}=(1+R)\frac{\partial^2\theta}{\partial y^2}+Nb\frac{\partial\phi}{\partial y}\frac{\partial\theta}{\partial y}+Nt\left(\frac{\partial\theta}{\partial y}\right)^2+G\theta+Df\frac{\partial^2\phi}{\partial y^2}+\Pr\frac{\alpha^{*2}Ra}{L^2C_p(T_f-T_\infty)}\left(1+\alpha^{-1}\right)\left(\frac{\partial^2\psi}{\partial y^2}\right)^2, \tag{18}$$

$$\frac{\partial\psi}{\partial y}\frac{\partial\phi}{\partial x}-\frac{\partial\psi}{\partial x}\frac{\partial\phi}{\partial y}=\frac{1}{Le}\frac{\partial^2\phi}{\partial y^2}+\left(\frac{Nt}{Nb}\frac{1}{Le}+Sr\right)\frac{\partial^2\theta}{\partial y^2}-\gamma\phi, \tag{19}$$

subjected to

$$\begin{cases} \dfrac{\partial\psi}{\partial y}=0,\ \ \dfrac{\partial\theta}{\partial y}=-\dfrac{Lh_f(x)}{kRa^{\frac{1}{4}}}(1-\theta),\ \ \phi=1,\ \ at\ \ y=0, \\ \dfrac{\partial\psi}{\partial y}\to 0,\ \ \theta\to 0,\ \phi\to 0,\ \ as\ \ \ y\to\infty. \end{cases} \tag{20}$$

Using equation (21) to transform equations (17)–(19) and the boundary conditions (20)

$$\eta = \frac{y}{x^{\frac{1}{4}}}, \psi = x^{\frac{3}{4}} f(\eta), \theta = \theta(\eta), k_p = x^{\frac{1}{2}}(k_p)_0, h_f(x) = x^{\frac{1}{4}}(h_f)_0, b^* = x^{-\frac{1}{2}}(b^*)_0 . \tag{21}$$

Resulted to systems of ordinary equations:

$$\left(1+\alpha^{-1}\right) f''' + \frac{1}{4\,\mathrm{Pr}}\left[3ff'' - 2f'^2 - 4(H+B)f'^2\right] + \theta - Nr\phi - \frac{1}{Da}\left(1+\alpha^{-1}\right) f' = 0, \tag{22}$$

$$\left(1+R\right)\theta'' + \frac{3}{4} f\theta' + Nb\phi'\theta' + Nt\theta'^2 + G\theta + Df\phi'' + \mathrm{Pr}\,Ec\left(1+\alpha^{-1}\right) f''^2 = 0, \tag{23}$$

$$\phi'' + \frac{3}{4} Lef\phi' - Le\gamma\phi + \left(\frac{Nt}{Nb} + LeSr\right)\theta'' = 0, \tag{24}$$

with the boundary conditions

$$\begin{cases} f'(\eta) = 0,\ f(\eta) = 0,\ \theta'(\eta) = -Bi(1-\theta(\eta)),\ \phi(\eta) = 1,\ at\ \eta = 0, \\ f'(\eta) \to 0,\ \theta(\eta) \to 0,\ \phi(\eta) = 0 \text{ as } \eta \to \infty, \end{cases} \tag{25}$$

where

$$Da = \frac{(k_p)_0 Ra^{\frac{1}{2}}}{L^2}, B = \frac{(b^*)_0 L}{(k_p)_0}, Bi = \frac{(h_f)_0 L}{kRa^{\frac{1}{4}}},\quad Ec = \frac{\alpha^{*2} Rax^{-1}}{L^2 C_p (T_f - T_\infty)},\quad Ra = \frac{(1-C_\infty)(T_f - T_\infty)\beta_0 g L^3}{\alpha^* \nu}$$

are the Darcy number, Forchheimer parameter, Biot number, and Eckert and Rayleigh number respectively.

Sherwood number ($Sh_{\bar{x}}$) and Nusselt number ($Nu_{\bar{x}}$) are quantities of interest due to the applications in practical engineering and design. Following Uddin et al (2012), we defined as follow

$$Nu_{\bar{x}} = -\bar{x}\frac{\left(\frac{\partial T}{\partial \bar{y}}\right)_{\bar{y}=0}}{(T_f - T_\infty)}, \qquad \text{and} \qquad Sh_{\bar{x}} = -\bar{x}\frac{\left(\frac{\partial C}{\partial \bar{y}}\right)_{\bar{y}=0}}{(C_w - C_\infty)}. \tag{26}$$

Using equations (11) and (21) together with stream function ψ on the equation (26), we have

$$Ra_{\bar{x}}^{-\frac{1}{4}} Nu_{\bar{x}} = -\theta'(0),\ and,\ Ra_{\bar{x}}^{-\frac{1}{4}} Sh_{\bar{x}} = -\phi'(0), \tag{27}$$

we have equation (27) as the reduced Nusselt number and Sherwood number accordingly, and the local Rayleigh number is $Ra_{\bar{x}} = \frac{(1-C_\infty) g B_0 (T_w - T_\infty)\bar{x}^3}{\alpha^* \nu}$.

3. Solution Technique

The solutions to the non-linear, coupled, ODEs in equations (22)–(24) subjected to boundary equation (25) are obtained via collocation technique with Legendre polynomial as the basis function. The problem boundary is $[0,\infty)$, to implement this numerical method, the domain is first truncated using the domain truncation approach $[0,L]$. The Legendre polynomial defined on $[-1,1]$ transformed to $[0,L]$ via algebraic mapping,

$$\omega = \frac{2\eta}{\mathrm{L}} - 1, \qquad \omega \in [-1,+1]. \tag{28}$$

The unknown function $f(\eta)$, $\theta(\eta)$, and $\phi(\eta)$ are approximated by the sum of a finite series of the legendary polynomial (P_j) as

$$\begin{aligned} f(\eta) &\cong f_N(\omega) = \sum_{j=0}^{N} a_j \left(\frac{2\eta}{L} - 1\right) P_j, \\ \theta(\eta) &\cong \theta_N(\omega) = \sum_{j=0}^{N} b_j \left(\frac{2\eta}{L} - 1\right) P_j, \qquad \text{for} \qquad j=0,1,...,N, \\ \phi(\eta) &\cong \phi_N(\omega) = \sum_{j=0}^{N} c_j \left(\frac{2\eta}{L} - 1\right) P_j, \end{aligned} \tag{29}$$

$f(\omega)$, $\theta(\omega)$ and $\phi(\omega)$ are approximate functions $f(\eta)$, $\theta(\eta)$ and $\phi(\eta)$ respectively at N discrete points, and a_j, b_j and c_j are the unknown constants to be determined. The generated equations of $3N+3$ algebraic systems with $3N+3$ unknown coefficient is solved via a MATHEMATICA symbolic package with newton iteration technique to simulate the system of derived algebraic equations to obtain the required constants coefficients (a_j, b_j and c_j). Hence, solutions are obtained for the flow distributions and flow characteristics $f'(\eta)$, $\theta(\eta)$ and $\phi(\eta)$ profiles.

4. Results and Discussions

Chebyshev collocation technique with a legendary basis function is implemented on the heat and mass transfer blood rheological model over a vertical plate. Considering the fluid characteristics, the following pertinent parameters, $\alpha = H = Bi = 0.5, Df = 0.01, Sr = 0.3, G = 0.01, \gamma = 0.2,$ $Da = Le = 1, \quad Pr = 0.71, \quad R = Ec = Nb = Nt = B = 0.1.$ (Uddin, Gbadeyan) are kept constant except otherwise stated.

Table 1: Comparison of Collocation and Runge-Kuta 4^{th} order method for Nusselt number with different values of $H, Pr, R, Ec, G, Df, Sr, and\ Le$

H	Pr	R	Ec	G	Df	Sr	Le	Collocation	R-K 4^{th} order
0.5	0.71	0.1	0.1	0.01	0.01	0.3	1.0	0.12067	0.12067
0.0	0.71	0.1	0.1	0.01	0.01	0.3	1.0	0.12024	0.12024
0.5	1.0	0.1	0.1	0.01	0.01	0.3	1.0	0.12035	0.12035
0.5	0.71	0.5	0.1	0.01	0.01	0.3	1.0	0.11704	0.11704
0.5	0.71	0.1	0.5	0.01	0.01	0.3	1.0	0.11372	0.11372
0.5	0.71	0.1	0.1	0.03	0.01	0.3	1.0	0.10116	0.10116
0.5	0.71	0.1	0.1	0.01	0.05	0.3	1.0	0.11282	0.11282
0.5	0.71	0.1	0.1	0.01	0.01	0.6	1.0	0.12067	0.12067
0.5	0.71	0.1	0.1	0.01	0.01	0.3	3.0	0.11869	0.11869

Tables 1 and 2 presents the comparative analysis of the Chebyshev collocation techniques, the first, with R-K 4^{th} order along with shooting techniques, and the latter with the work of Uddin, where shooting technique along with Runge-Kutta-Fehlberg forth-fifth order method was employed. A good agreement of the numerical result is found. Therein Table 2, a rise in Pr the showcase its ability to promote heat transfer rate at the flow surface. Physically, heat diffuses away more rapidly since the rise Pr is relative to high thermal conductivity. However, a downsizing behavior of heat transfer rate is experienced to higher Nb and Nt as a result of stronger thermophoretic force which drags the nanoparticles from the nanofluid to the wall surface and leads to a reduction, as perceived.

Numerical simulation results for Nulset number and Sharwood number for distinct pertinent parameters are recorded in Table 3. It is noticed that a hike in Df, G and γ slows down the energy transfer and speedup the mass transfer at the wall. Influence of other quantities considered as depicted in the table. The influence of flow parameters such as Soret, Doufor, Casson, Heat source, Chemical reaction among others on the flow configuration is presented graphically in Figures 2 - 13.

Table 2: Comparison of Uddin et al. (2012) and present results of Nusselt number for $H = B = R = Ec = G = Df = Sr = \gamma = 0, \quad Nt = Nb = 0.1, \quad Le = Bi = 10, Da \to \infty, \alpha \to \infty$

		Pr = 1		Pr = 5		Pr = 10	
Nb	Nr	Uddin et al. (2012)	Present	Uddin et al. (2012)	Present	Uddin et al. (2012)	Present
0.1	0	0.34257	0.34257	0.38395	0.38375	0.39530	0.39468
0.1	0.2	0.33659	0.33659	0.37734	0.37716	0.38856	0.38797
0.1	0.4	0.33012	0.33013	0.37024	0.37007	0.38133	0.38075

0.3	0.0	0.2960	0.29599	0.33288	0.33269	0.34301	0.24246
0.3	0.2	0.29178	0.29177	0.32821	0.32804	0.33826	0.33774
0.3	0.4	0.28724	0.28724	0.32322	0.32308	0.33319	0.33270

Table 3: Computational values of Sherwood number and Nusselt number $Df, Sr, G, \gamma, Ec, R, H, Bi, Da$, and Le.

D_f	S_r	G	γ	Ec	R	H	Bi	Da	Le	$-\theta'(0)$	$-\phi'(0)$
0.01	0.3	0.01	0.2	0.1	0.1	0.5	0.5	1.0	1.0	0.12067	0.47632
0.05	0.3	0.01	0.2	0.1	0.1	0.5	0.5	1.0	1.0	0.11282	0.48774
0.01	0.6	0.01	0.2	0.1	0.1	0.5	0.5	1.0	1.0	0.12067	0.47543
0.01	0.3	0.03	0.2	0.1	0.1	0.5	0.5	1.0	1.0	0.10116	0.50266
0.01	0.3	0.01	0.6	0.1	0.1	0.5	0.5	1.0	1.0	0.11887	0.80230
0.01	0.3	0.01	0.2	0.5	0.1	0.5	0.5	1.0	1.0	0.11372	0.48800
0.01	0.3	0.01	0.2	0.1	0.5	0.5	0.5	1.0	1.0	0.11704	0.47757
0.01	0.3	0.01	0.2	0.1	0.1	1.0	0.5	1.0	1.0	0.12024	0.47629
0.01	0.3	0.01	0.2	0.1	0.1	0.5	1.0	1.0	1.0	0.14265	0.47591
0.01	0.3	0.01	0.2	0.1	0.1	0.5	0.5	5.0	1.0	0.14342	0.48064
0.01	0.3	0.01	0.2	0.1	0.1	0.5	0.5	1.0	3.0	0.11869	0.83801

Figures 2(a and b) indicate the dominance of Df on fluid velocity and temperature profiles respectively. Effects of Df clearly point out the role of composition gradients presented in Equation (23). This effect is however attributed to playing an essential part due to its ability to elevate the thermal energy and assisting the fluid flow process. Rise in Df has a positive influence on both temperature and velocity fields. Figure 3 presents the variations of Sr on the nanofluid volume fraction ($\phi(\eta)$). The fluid concentration far away from the wall plate is seen to rise gradually to an appreciable value Sr. This is ascribed to a higher ratio of Sr to that of thermal diffusion. Hence, a raise Sr increases the fluid concentration.

Uplifting H generates Lorentz force perpendicular to the flow path which corresponds to the retarding force thus resulted in momentum boundary layer reduction as depicted in Figure 4. A corresponding rise in Radiation effect (R), fluid motion, and energy field is pictured in Figures 5(a) and 5(b) accordingly. Physically, thermal boundary layer thickness, fluid temperature, and hydrodynamic are enhanced to a growth in radiative heat which is discharged into the flow system, thus elevate the fluid velocity and temperature.

A transformation of kinetic energy into heat energy via the work done by the fluid molecules which take place influences both dimensionless velocity and temperature significantly. These are

perceived appreciating with increasing values of Ec as pictured in Figures $6a$ and $6b$. A higher γ appreciates the momentum distribution, lessening the nanoparticle volume fraction as depicted in Figures $7a$ and $7b$ respectively.

Impact of Darcian drag force parameter (B), Darcy number (Da) over momentum profile is highlighted in Figures $8a$ and $8b$ respectively. Mathematically, $B \propto 1/Da$ as presented in Equation (22) however, a hike in B depreciating fluid velocity while a rise in Da appreciating the momentum boundary layer.

In Figures 9(a and b), the heat generated by the intermolecular reaction of fluid particles resulted in large amount of heat produced. Thus, the velocity and temperature fields are enhanced to an appreciable value G. The effect of the base fluid (Casson) α is depicted in Figure 10, on velocity profiles. Physically, a rise in α result to a reduction in yield stress thus appreciates the fluid velocity and boundary layer thickness as presented in Figure 10. Higher magnitude Bi gave appreciable profiles for both temperature and velocity as indicated in Figures 11(a and b) accordingly. This is due to convective heating enhancement at the wall.

Nanoparticle parameters Nt and Nb impacts are presented in Figures 12 and 13. Figures 12(a and b) elucidates temperature and concentration profiles to an effect of Nb respectively. Notably, the collision of the nanofluid particles caused by an increase in Nb generating thermal energy which speedup the temperature distribution (see $12a$), concentration field gave an opposing characterization as presented in Figure $12b$. Figure 13 displayed the impact of thermophoresis on $\phi(\eta)$. Clearly, a hike Nt leads to a rise in nanoparticle volume fraction.

5. Conclusion

In this section, we discussed the Soret-Dufour influence in MHD blood rheological motion of nanofluid encompassing mass transfer, radiative, heat, convective heating, chemically reacting, and dissipative flow past a vertical plate. Dimensional PDEs which governed the flow is transformed to coupled nonlinear ODEs, using appropriate similarity variable. These equations are approximated via Chebyshev collocation techniques with a legendary basis function. The solution technique is seen to give an excellent approximation as seen in Tables 1 and 2. Thus, the following conclusions are highlighted.

1. The velocity is appreciated with a rise in Bi, G, α, γ and Df while depreciation is observed for an increase in H and B.
2. An increase in $Bi, G,$ and Df speedup temperature profiles of Casson nanofluid.
3. Concentration profiles rise with Sr and Nt while an opposite behavior is perceived for

appreciable values of γ and Nb.

4. At the wall, an increase in Df, G, and γ appreciated mass transfer and diminished the rate of energy transfer.

REFERENCES

Akolade, M. T., Adeosun, T. S. and Olabode, J.O. (2020). Influence of Thermophysical Features on MHD Squeezed Flow of Dissipative Casson fluid with Chemical and Radiative Effects, J. Appl Comp. Mech., Vol-,No-, pp. -. doi: 10.22055/jacm.2020.34909.2508.

Akolade, M. T., Idowu, A. S. and Adeosun, T. S. (2021). Multi-Slip and Soret-Doufur Influence on non-linear Convection Flow of MHD Dissipative Casson Fluid Over a Slendering Stretching Sheet with Modified heat Flux Phenomenon. Heat Transfer Res., , Vol-, No-, pp. - DOI: 10.1002/htj.22057

Alao F.I., Boneze C.U. and Fagbade A.I. (2019) Soret and Dufour effects on heat and mass transfer of boundary layer flow over porous wedge with thermal radiation: Bivariate spectral relaxation method. American Journal of chemical Engineering, Vol. 7, No. 1, pp. 7–21.

Ali A., Iqbal F., Khan D.N.M., Asghar S. and Awais M., (2019) Soret and Dufour effects between two rectangular plane walls with heat source/sink. Heat transfer Res., Vol. 49, pp. 614–625.

Ali A., Sajjad A. and Asghar S. (2019). Thermal-diffusion and Diffusion-thermo effects in a nanofluid flow with non-uniform heat flux and convective walls, J. Nanofluids, Vol. 8, pp. 1367–1372.

Animasaun I.L. (2015). Effect of thermophoresis, variable viscosity and thermal conductivity on free convective heat and mass transfer of non-darcian MHD dissipative Casson fluid flow with suction and n^{th} order chemical reaction, Journal of Nigeria Mathematical Society, Vol. 34, pp. 11–31.

Arthur E.M., Seini Y.I. and Antwi D.G. (2015). Analytical solution of Dufour and Soret effects on hydro magnetic flow past a vertical plate embedded in a porous medium, Advances in Physics Theories and Applications, Vol. 44, pp. 47–71.

Chaoyang W. and Chuanjing T.U. (1989). Boundary-layer flow and heat transfer of non-Newtonian fluids in porous medium. Int. J. Heat fluid flow. Vol. 10, No. 2, pp. 160–165.

Finlayson, B. A. (1972). *The Method of Weighted Residuals and Variational Principles* Academic Press, New York.

Gbadeyan J.A., Oyekunle T.L., Fasogbon P.F. and Abubakar J.U. (2018) Soret and Dufour effects on heat and mass transfer in chemically reacting MHD flow through a wavy channel. Journal of Taibah University for Sci., Vol. 12, No. 5, pp. 631–651

Gbadeyan J.A., Titiloye E.O and Adeosun A.T. (2020). Effct of variable thermal conductivity and viscosity on Casson nanofluid flow with convective heating and velocity slip, Heliyon, Vol. 1, No. 6, pp1–10, https//doi.org/10.1016/j.heliyon.2019.e03076

Gireesha B.J., Krishnamurthy M.R., Prasannakumara B.C. and Rama S.R. (2018). MHD flow of nonlinear radiation heat transfer of a Casson nanofluid past a nonlinear stretching sheet in the

presence of chemical reaction. Nanoscience and technology: An International Journal, Vol. 9, No 3, pp. 207–229.

Haroun N.A., Sibanda P., Mandal S. and Motsa S.S. (2015). On unsteady MHD mixed convection in a nanofluid due to a stretching /shrinking surface with suction/injection using the spectral relaxation method. Boundary Val. Probl., Vol. 1, pp. 1–17, http://dx.doi.org/10.1186/s13661-05-0289-5.

Turkyilmazoglu M. (2015). Natural Convective Flow of Nanofluids Past a Radiative and Impulsive Vertical Plate. J. Aerosp. Eng., pp. 1–8, 04016049, DOI: 10.1061/(ASCE)AS.1943-5525.0000643.

Turkyilmazoglu M. (2010). The MHD boundary layer flow due to a rough rotating disk, ZAMM. Z. Angew. Math. Mech. Vol. 90, No. 1, pp. 72–82. DOI 10.1002/zamm.200900259

Turkyilmazoglu M. (2012). Effects of uniform radial electric field on the MHD heat and fluid flow due to a rotating disk, International Journal of Engineering Science, Vol. 51, pp. 233–240.

Turkyilmazoglu M. (2019). MHD natural convection in saturated porous media with heat generation/absorption and thermal radiation: closed-form solutions, Arch. Mech. Vol. 71, No. 1, pp. 49–64, DOI: 10.24423/aom.3049

Idowu A.S. and Falodun B.O. (2019) Soret-Dufour effects on MHD heat and mass transfer of water's B viscoelastic fluid over a semi-infinite vertical plate.: spectral relaxation analysis, Journalof Taibah Univ. Sci., Vol. 13 No. 1, pp. 49–62

Idowu A.S. and Falodun B.O. (2020a). Effects of thermophoresis, Soret-Dufour on heat and mass transfer flow of MHD non Newtonian nanofluid over an inclined plate. Arab Journal of Basic and Applied Scciences, Vol. 27, No. 1, pp. 149–165

Idowu A.S., Akolade M.T., Abubakar J.U. and Falodun B.O. (2020b). MHD free convective heat and mass transfer flow of dissipative Casson fluid with variable viscosity and thermal conductivity effects. Journal of Taibah University for Sci., Vol. 14, No. 1, pp. 851–862, https://doi.org/10.1080/16583655.2020.1781431

Idowu A. S., Akolade M.T., Oyekunle T.L. and Abubakar J.U., (2020c). Nonlinear convection flow of dissipative Casson nanofluid through an inclined annular microchannel with a porous medium. Heat Transfer, Res. Vol. -, No.-, pp. 1â€“19. https://doi.org/10.1002/htj.22033

Jawad R., Azizah M. and Zurn O. (2016). Multiple solution of mixed convective MHD Casson fluid flow in a channel. Journal of Applied Mathematics, Vol. 2016, pp 1–10, http://dx.doi.org/10.1155/2016/7535793.

Kafoussias N.G. and Williams E.W. (1995) Thermal-diffusion and Diffusion-thermo effects on mixed free forced convection and mass transfer boundary layer with temperature dependent viscosity. Int. J. Eng.Sci., Vol. 33, pp. 1369–1384

Kaladhar K., Komuraiah E. and Reddy K.M. (2019) Soret and Dufour effects on chemically reacting mixed convection flow in an annulus with navier slip and convective boundary conditions, Applied Mathematics and nonlinear sciences, Vol. 4, No. 2, pp. 475–488

Oyelakin I.S., Mondal S. and Sibanda P. (2016). Unsteady Casson nanofluid flow over a stretching sheet with thermal radiation, convective and slip boundary condition. Alexandria Engineering Journal, Vol. 55, No. 2, pp. 1025–1035

Rafique K., Anwar M.I., Misiran M., Khan I., Alharbi S.O., Thounthong P., and Nisar K.S. (2019). Numerical solution of Casson fluid flow over a nonlinear inclined surface with Soret and Dufour effects by Keller- Box method. Frontier Physics, Vol. 7, No. 139, pp. 1–13. doi:10.3389/fphy.2019.00139

Rajasekhar N.S., Prasada P.M.V., and Prasada Rao D.R.V. (2013). Effect of chemical reaction and radiation absorption on unsteady convective heat and mass transfer flow of a viscous electrically conducting fluid in a vertical wavy channel with travelling thermal waves and Hall effects. Int. J. Engr. Res. and Applic. Vol. 3, No. 1, pp. 1733-1747

Raju C.S.K., Sandeep N., Sugunamma V., Jayachandra M.B. and Ramana R.J.V. (2016). Heat and mass transfer in MHD Casson fluid over an exponentially permeable stretching surface,Engineering Science and Technology, an International Journal, Vol. 19, No. 1, pp. 45-52

Raju R.S., Reddy G.J., Rao J.A., Rashidi M.M. (2016) Thermal-diffusion and Diffusion-thermo effects on an unsteady heat and mass transfer MHD natural convection coquette flow using FEM.Journal of computational Desgn and Engineering, Vol. 3, pp. 349–362

Uddin M. J., Khan W. A. and Ismail A. I. (2012). MHD free convective boundary layer flow of a nanofluid past a flat vertical plate with Newtonian heating boundary condition. PLOS ONE, Vol. 7, No. 11, pp. 1–8, e49499.doi:10.1371/ journalpone.0049499.

Ullah I., Khan I. and Shafie S. (2017) Soret and Dufour effect on unsteady mixed convective slip flow of Casson fluid over a nonlinearly stretching sheet with convective boundary condition. Scientific report, Vol. 7, pp. 11–13 doi:10.1038/s41598-017-01205-5

Appendix

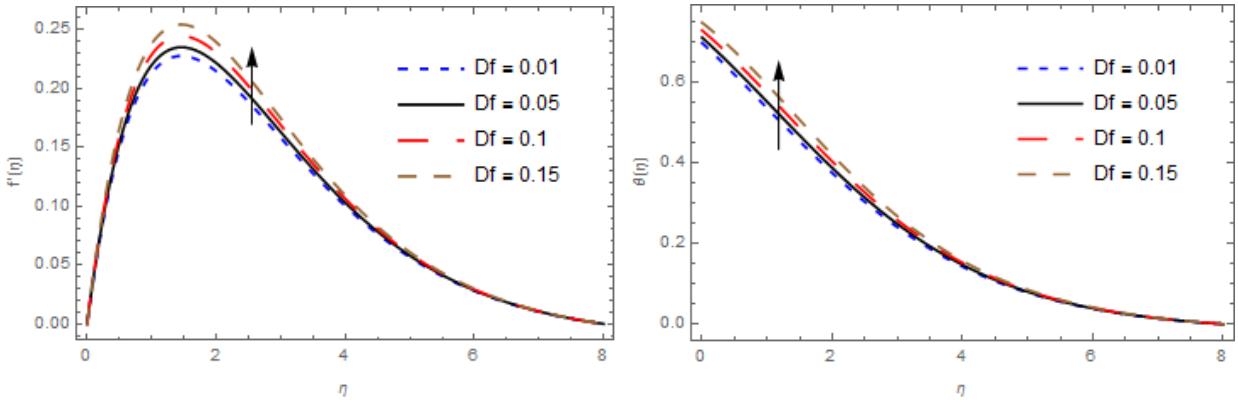

(a) (b)

Figure 2: Impact of Dufour number (Df) on (a) velocity, (b) temperature.

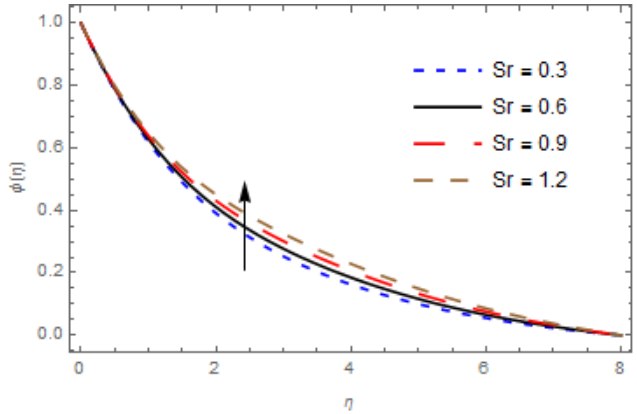

Figure 3: Impact of Soret number (Sr) on concentration.

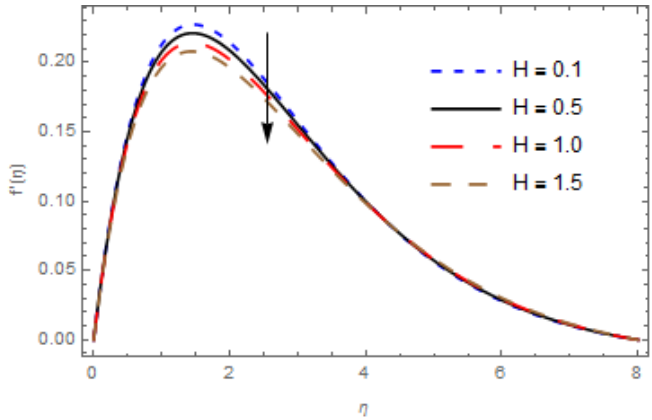

Figure 4: Impact of Magnetic field (H) on velocity.

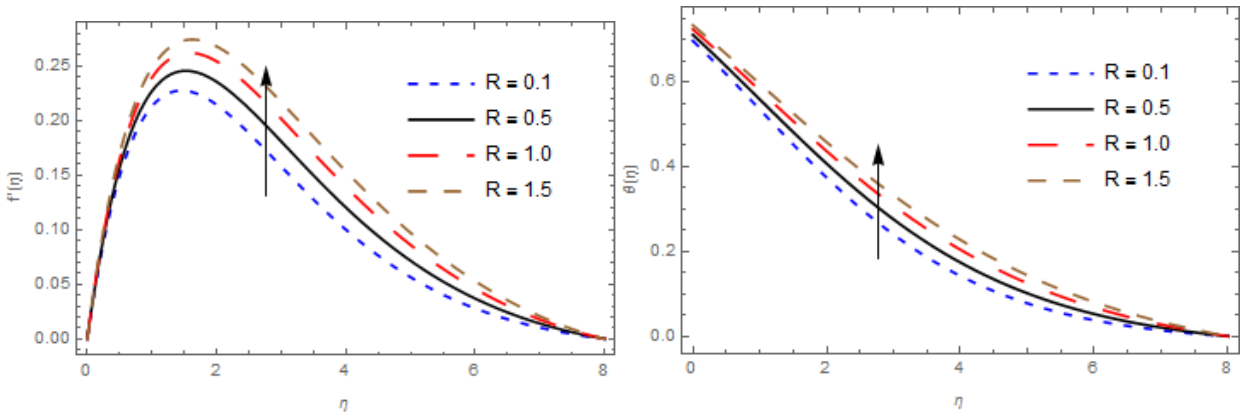

(a) (b)

Figure 5: Impact of Radiation (R) on (a) velocity, (b) temperature.

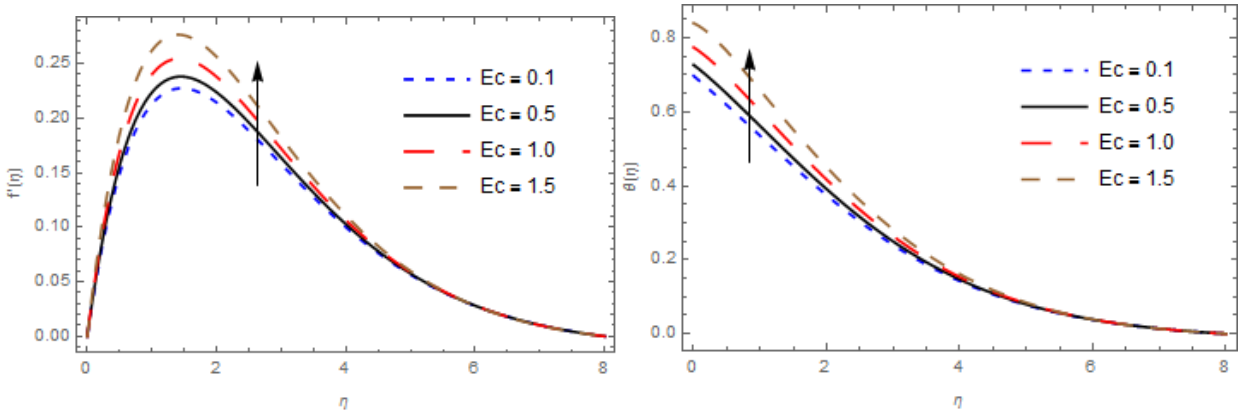

(a) (b)

Figure 6: Impact of Eckert number (Ec) on (a) velocity, (b) temperature.

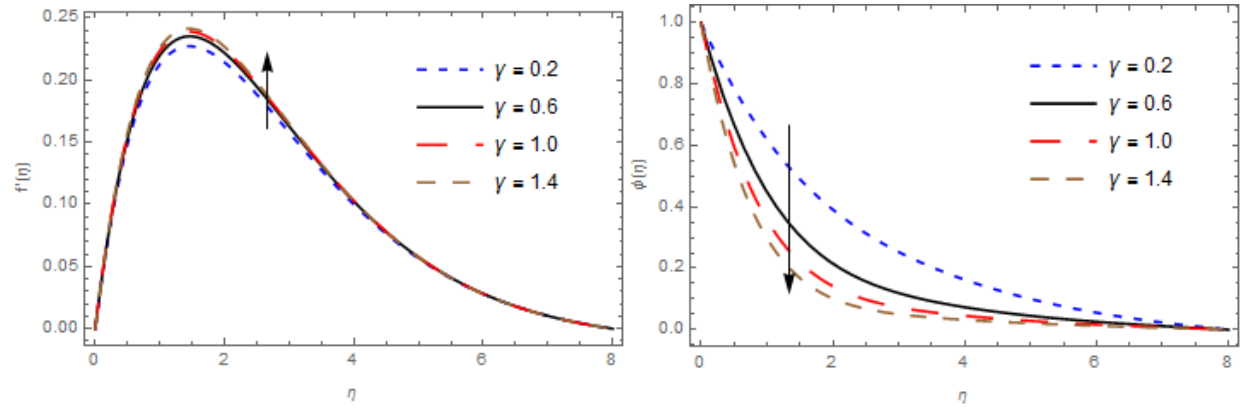

(a) (b)

Figure 7: Impact of chemical reaction (γ) on (a) velocity, (b) concentration.

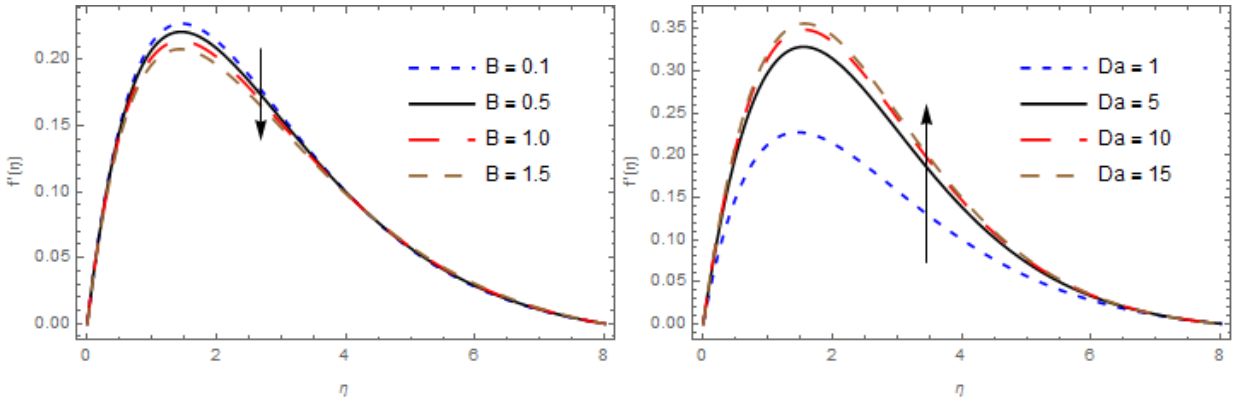

(a) (b)

Figure 8: Impact of (a) Darcian drag force (B), (b) Darcy number (Da) on velocity.

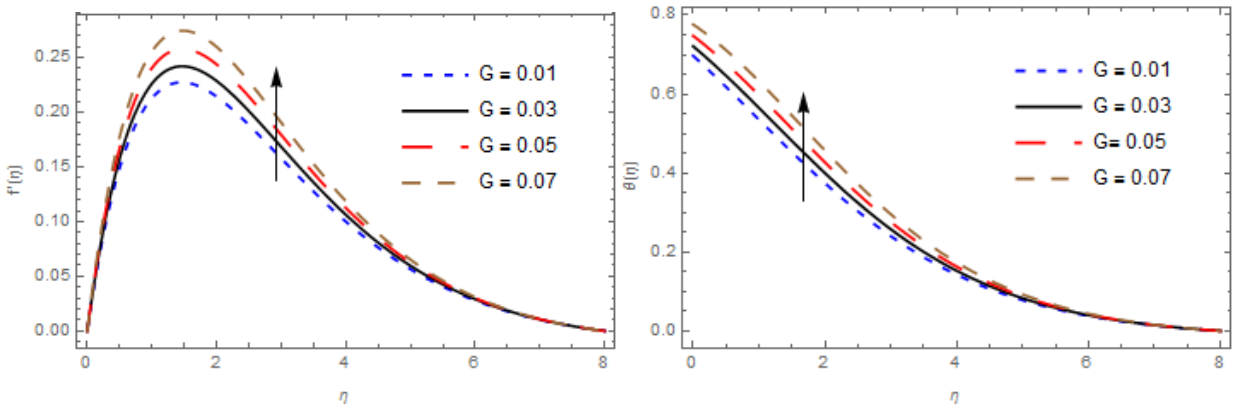

(a) (b)

Figure 9: Heat generation (G) impact on (a) velocity, (b) temperature.

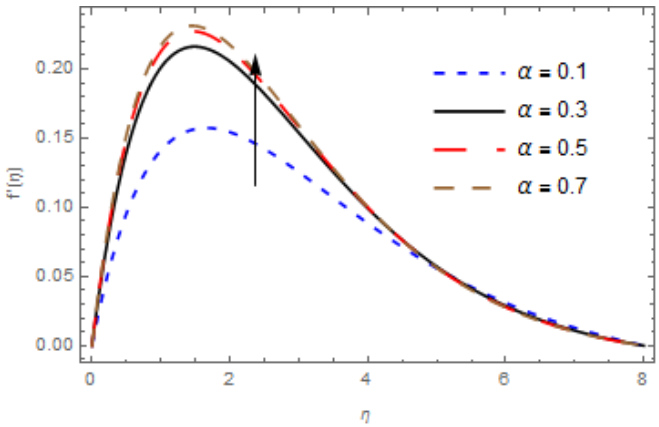

Figure 10: Casson rheological impact (α) on the velocity field.

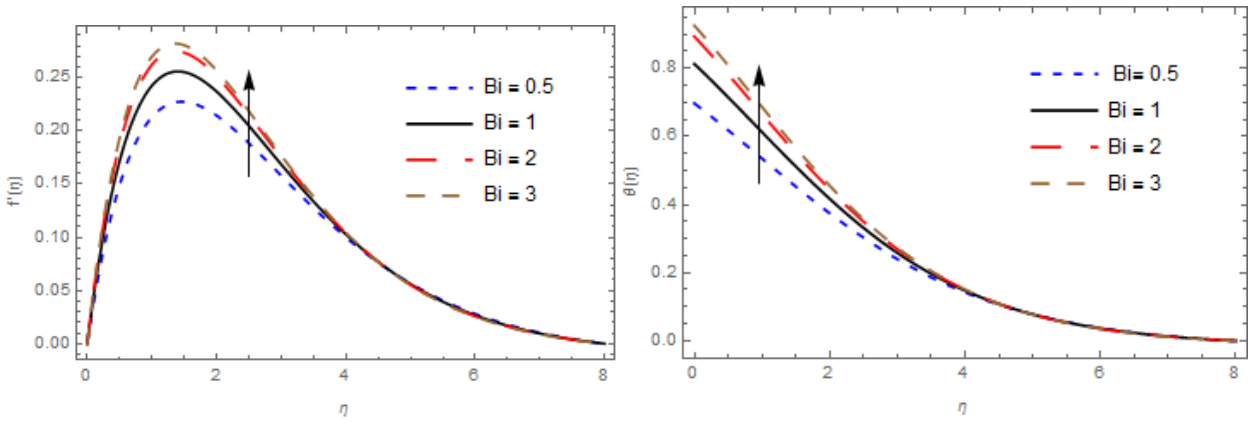

(a) (b)

Figure 11: Biot parameter (Bi) influence on (a) velocity, (b) temperature.

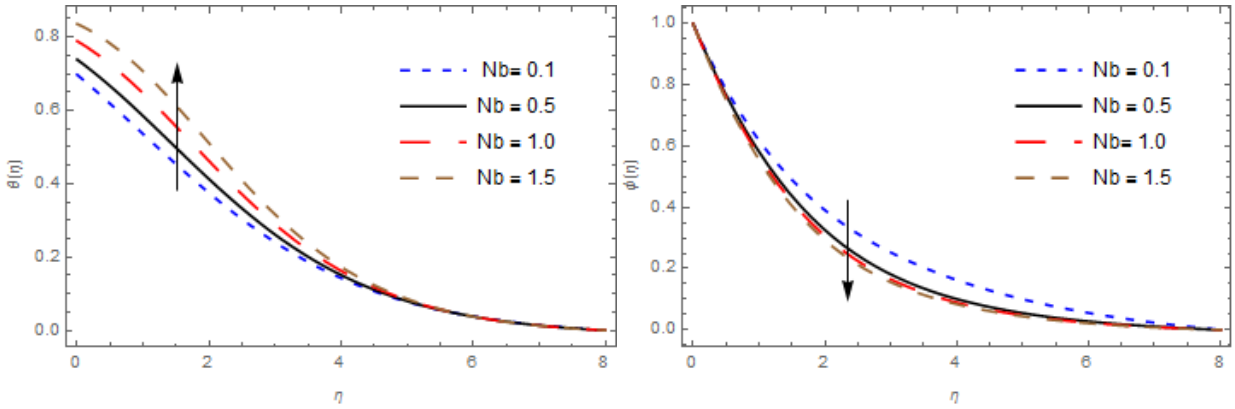

(a) (b)

Figure 12: Brownian motion impact on (a) temperature, (b) concentration.

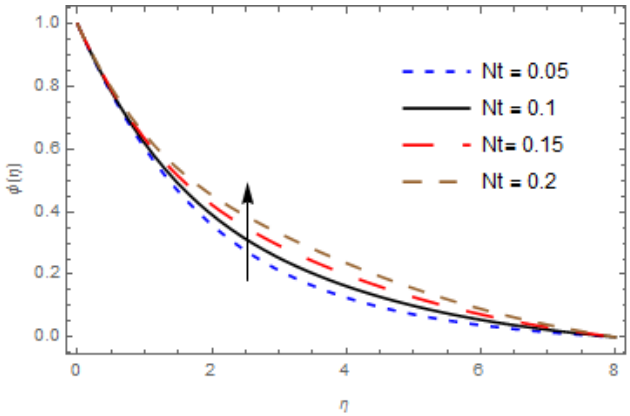

Figure 13: Thermophoresis effect (Nt) on concentration.